

Dielectric breakdown along c-axis boundaries in magnetoelectric Cr₂O₃ for spintronic devices

Congli Sun¹, Zhewen Song¹, Michael Street², William Echtenkamp², Jie Feng¹, Christian Binek², Dane Morgan¹, Paul M. Voyles¹

¹. Department of Materials Science and Engineering, University of Wisconsin-Madison, Madison, WI, 53706, USA

². Department of Physics and Astronomy, Nebraska Center for Materials and Nanoscience, University of Nebraska, Lincoln, Nebraska 68588, USA

Voltage controlled boundary magnetism is crucial for spintronic devices with reduced power consumption. Magnetoelectric and antiferromagnetic Cr₂O₃ is an ideal material due to its electric field switching of nonvolatile boundary magnetism [1]. The boundary magnetization can switch an adjacent soft ferromagnetic layer via voltage-controlled exchange bias. Bulk Cr₂O₃ has a high dielectric breakdown field of 1000 KVmm⁻¹ and a large bandgap of 3.4 eV. However, even with a small electrode size of 0.04 mm² and thick Cr₂O₃ film of 0.5 μm, the highest reported dielectric breakdown field of Cr₂O₃ films is only 200 KVmm⁻¹ [2]. The breakdown field drops rapidly to 8 KVmm⁻¹ if electrode size increases to 35 mm² and film thickness decreases to 250 nm [2], making electric field induced switching of Cr₂O₃ based heterostructures very difficult. Here, we combine aberration corrected STEM characterization and spin polarized density functional theory (DFT) calculations to elucidate the structure, electronic properties, and magnetic properties of a new type of interface-stabilized planar crystallographic defect in Cr₂O₃ thin films that explains the structural origin of dielectric breakdown.

Figure 1(a) is a low-angle annular dark field (LAADF, 35-150 mrad) STEM image of a Cr₂O₃ film on Al₂O₃ substrate. LAADF is sensitive to strain fields [3], so the image emphasizes the columnar boundaries along the c-axis. The inset in Figure 1(a) is a high-angle ADF (HAADF, 84-165 mrad) STEM image along one of the boundaries. The HAADF signal scales as Z^a , so this image is dominated by Cr sites, and the oxygen atoms are invisible. Figure 1(b) is a plan view HAADF STEM (54-160 mrad) image. This intermediate range of scattering angles was used to mix sensitivity to both boundary strain field and Z-contrast of Cr sites on the boundary, so along the plan view axis the boundaries are imaged edge-on as narrow bright lines superimposed on the Cr₂O₃ lattice. The inset in Figure 1(b) shows the magnified boundary area with a boundary model constructed based on the plan view and cross section STEM images. Cr has an ABC stacking order along the c-axis and is marked by solid symbols with a different color for each layer. The boundary structure can be described as a 60° rotation about the c-axis, plus a shift of $\frac{1}{3}[10\bar{1}0]$ parallel to the basal plan to match the Cr plan view symmetry. The boundary model matches with the DFT calculation of the Cr₂O₃/Al₂O₃ interface defect grains. Figure 1(c) is the relaxed boundary model from spin polarized DFT calculations. A multi-slice STEM simulation from the model is superimposed on the inset of Figure 1(a). In DFT, the boundary model shows continuous boundary spins that do not interrupt the surface magnetization utilized for exchange bias switching in devices.

Figure 2(a) is O K edge extracted from EEL spectrum images on the boundary. It shows an O pre edge feature that only exists only locally on the boundary. Multiple scattering EELS simulation from the DFT model with FEFF9.6 reproduces the pre-edge. As the O-K edge reflects the portion of the conduction band projected onto O atoms, the additional peak is an indication of a reduced bandgap on the boundary arising from O unoccupied 2p states. The reduced bandgap energy is also confirmed by density of states

calculations, as shown in Figure 2(b). Breakdown voltage is roughly proportional to bandgap energy raised to a characteristic power, so, the c-axis boundaries with reduced bandgap energy in the $\text{Cr}_2\text{O}_3/\text{Al}_2\text{O}_3$ thin film systems are likely to create local easy breakdown paths.

References:

- [1] X. He, Y. Wang, N. Wu, et al., *Nat. Mater.* 9 (2010) 579–85.
- [2] T. Ashida, M. Oida, N. Shimomura, et al., *Appl. Phys. Lett.* 106 (2015) 132407.
- [3] A. Mosk, D. A. Muller, N. Nakagawa, et al., *Nature* 430 (2004) 657.
- [4] This work was supported in part by C-SPIN, one of the six centers of STARnet, a Semiconductor Research Corporation program, sponsored by MARCO and DARPA.

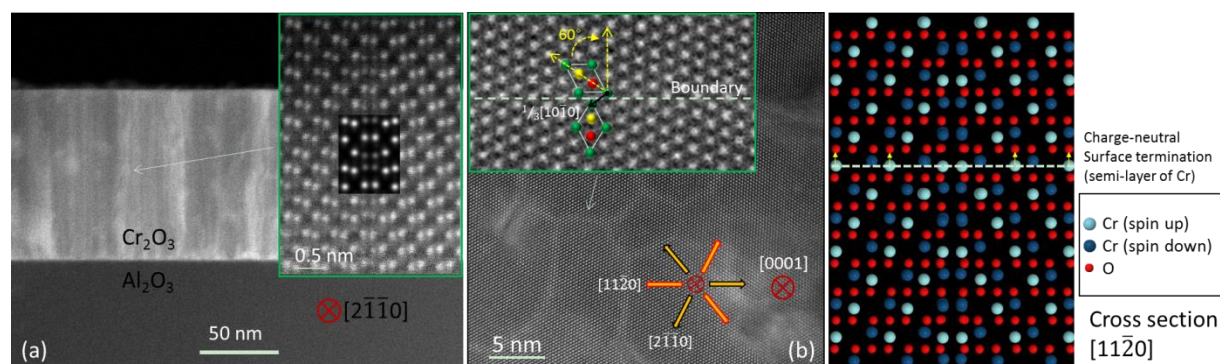


Figure 1. (a) Cross-section LAADF STEM image of $\text{Cr}_2\text{O}_3/\text{Al}_2\text{O}_3$ showing vertically aligned grain boundaries. The inset is HAADF STEM image of one of the boundaries, with multi-slice STEM simulation superimposed. (b) Plan-view HAADF STEM image. Inset is the magnified boundary image with structure model superimposed. Different color of balls represent the ABC ordered stacking layer of Cr along the c-axis. (c) Relaxed boundary model from spin polarized DFT calculations. The white dashed line is one of the stable charge-neutral surface terminations, showing continuous spin across the boundary.

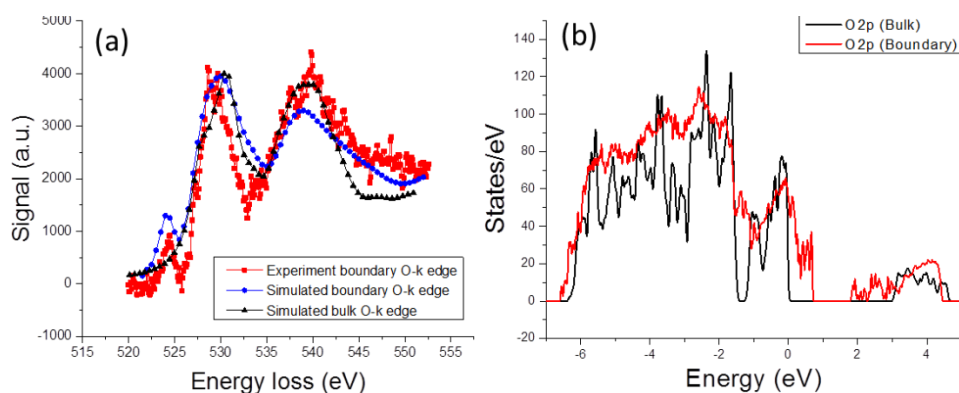


Figure 2. (a) Boundary O K edge showing a pre-edge and multiple scattering EELS simulations. (b) Density of states calculations showing that the pre-edge is inside the bandgap, reducing bandgap energy on the boundaries.